

# Intensity variations of small airborne incoming targets, popping-up above the horizon

Arie N. de Jong

TNO - Physics and Electronics Laboratory, The Hague – Netherlands

## ABSTRACT

The sensitivity of modern infrared sensors, using cooled Focal Plane Arrays (FPA's), allows the detection of small incoming airborne targets at sea as soon as they pop-up over the horizon. Experiments show strong fluctuations of the contrast-irradiance level of target and background at the entrance pupil of the sensor. The characteristics of these fluctuations have an impact on the design of detection- and tracking algorithms of Infrared Search and Track (IRST) sensors and tracking systems. Several physical phenomena may contribute to the apparent contrast intensity (and thus signal) variations, such as specular sun- or cold sky reflections at the target surface, changes in the aspect angle and height of the target, coherence of the target radiation dependent on its size and range, atmospheric turbulence, wave chopping, diffraction at the wave tops, wave effects on the temperature profile in the atmospheric boundary layer, local droplet clouds produced by breaking waves, detector temporal- and spatial noise and under-sampling and fill-factor effects when the sensor is panning over the scene. The magnitude of each of these effects is estimated and compared to data from measurements. It is in general not simple to determine which effect is dominant in a certain case. The low frequency behaviour of the signal variations suggests that "classical" scintillation is not the major contributor in most cases. It is shown that structure variations in the boundary layer along the path due to waves, may be responsible for most of the low frequency effects.

**Keywords:** atmospheric scintillation, atmospheric propagation, infrared, point target detection

## 1. INTRODUCTION

In this paper, phenomena occurring in a maritime scenario will be discussed. Small targets, flying and incoming at low altitude (between 3 and 30 m), are to be detected by means of infrared sensors on board of ships, mounted at a height between 10 and 30 m above sea level. It is of great operational importance that these targets can be detected as soon as possible with respect to potential counter-actions to be undertaken, especially when the targets are flying at supersonic speeds. A standard (and maximum) requirement, concerning the detection range is the horizon range, which implies detection as soon as the target pops-up over the horizon. This range is about 27 km when the sensor height is 20 m and the target height is 10 m, neglecting atmospheric refraction effects. Modern sensors, having a Noise Equivalent Irradiance (NEI) of 100 pW/m<sup>2</sup>, provide a signal to noise (S/N) ratio of about 7 for a target with a Radiant Intensity Contrast (RIC) of 10 W/sr and an atmospheric extinction coefficient of 0.1 km<sup>-1</sup>. In this case it is evident that the horizon range requirement is achieved. This implies that the light path between the target and the sensor is grazing the water surface and that propagation effects in the lowest part of the marine boundary layer are of key importance.

It is well known, that most of the time strong signal fluctuations are detected in the scenario just described. These fluctuations may disturb the detection process in classical IRST systems with low frame rates, as the signals in consecutive frames are nearly uncorrelated. However, high frame rate IRST's, using FPA's, may benefit from the signal fluctuations, on the one hand because they are specific for a small target with nearly coherent emission and do not occur in the background radiance, on the other hand because the IRST processor can make use of signal peak values, rising far above the average atmospheric transmission level [1]. As a consequence the performance of these new generation full stare IRST's in terms of lower false alarm rates and more range (better S/N ratio), exceeds considerably the performance of the classical alerting devices [2]. Also IR tracking devices, such as the ALBATROSS camera in the MIRADOR Trainable Electro-Optical Sensor System (TEOOS) on board of the new Air Defence Command Frigate of the Netherlands will benefit from the increased S/N ratio by using peak signal detection algorithms.

It is generally assumed that the most important phenomenon, causing signal fluctuations from point targets at long range, concerns scintillation as inherent to atmospheric turbulence. Beland [3] presents a theoretical model, in which the effect of turbulence is converted into small-scale temperature variations. These temperature variations are responsible for small variations in the refractive index of air, which in turn cause small wave-front distortions for a wave propagating from a target to a sensor. These phase distortions lead to changes in direction of the beam (beam wander) and interference effects at the detector. The parameters, generally used for the prediction of scintillation are the refractive index structure function  $C_N^2$ , which is proportional to the variance in the intensity fluctuations, measured by the detector and the atmospheric coherence length  $r_0$ , responsible for the time-dependent blurring. Recent performance models, such as IRTOOL [4], use this concept to predict signal fluctuations in various conditions such as wind speed and Air to Sea Temperature Difference (ASTD). Davidson [5] has set-up a model for calculating optical turbulence from atmospheric bulk parameters in maritime conditions. This model was further evaluated by Kunz [6] and examples were given of the effect of variations in each of the bulk parameters. Forand [7] developed a physical model, describing the influence of micro-meteorological parameters on optical effects like refraction and scintillation in the marine boundary layer. This Canadian LWKD model is part of the propagation model IRBLEM, used by various nations for prediction of optical propagation effects in a marine environment [8].

Various experiments have been carried out concerning scintillation effects on detection and tracking of long-range point targets at low altitudes over sea. Kunz [9] and de Leeuw [10] reported on experiments in the North Sea, during which a source was used at a fixed range of 19 km and at a variable height. Schwering [11] presented scintillation data on a point source, hanging under a helicopter in the North Sea area. Klein [12] compared data, measured with a source on a boat on the Atlantic ocean near Maryland, with the model described by Beland. Marable [13] reported on the impact of these results on IRST performance. Their conclusion on performance reduction by scintillation for low frame rate IRST's, was opposite to the conclusion by de Jong [1], valid for high frame rate IRST's. Beaumont [14] presented results on measurements of atmospheric Point Spread Functions (PSF) over-water. From the measured blur he could determine the value of  $r_0$ . De Jong [1, 15, 16, 17, 18] presented results from a variety of measurement campaigns. Various types of sources were used: non-modulated or modulated, mounted fixed on a pier or a boat, moving in and out beyond the horizon. He found always scintillations for ranges of more than 15 km, even when air and sea have the same temperature and when the  $C_N^2$  has very low values. Takken [19] carried out measurements near Monterey with a point source, similar to that of Schwering [11], under a helicopter and investigated the effects of scintillation and wave-chopping while the source was located just at the apparent horizon. Direct measurement of turbulence includes the use of a buoy, located mid-path, provided with a meteo-station including a sonic anemometer, measuring the wind-speed in three orthogonal directions. Frederickson [20] points out that a reasonable agreement exists between the  $C_N^2$  obtained in this way from the bulk parameters and high-speed transmissometry over a 7 km path in the San Diego bay. Similarly results from Germany and Canada on  $C_N^2$  measurements obtained simultaneously with a standard scintillometer and a sonic anemometer during a two-week period over a 2 km path in a Mediterranean coastal environment show quite good agreement [18].

This paper presents results from recent IR experiments, carried out with near horizon point targets at long range (more than 15 km), showing effects, not easy to explain with just scintillation theory. It is noted that the theory is limited to certain maximum wave-front distortions, set by the Rytov approximation [3]. The long ranges imply much larger wave-front deviations than half a wavelength, even for the IR wavebands (around 4 and 10  $\mu\text{m}$ ). In practice it appears, that for a series of images, the target will disappear completely (zero contrast), while other frames in the same series may provide apparent intensities exceeding the free space intensity. The image formation is entering the zone of saturation for these cases. Other uncertainties in the theory are the assumptions concerning the value of the atmospheric parameters and the neglecting of their variations along the path. In coastal areas the marine boundary layer is furthermore affected in the case of offshore winds, causing large ASTD's implying large  $C_N^2$ 's. The finite dimensions of the target and the sensor-aperture have an impact on the beam width, resulting in possible variations of the temperature gradient over the beam. Special attention will be spent on the low-frequency behaviour in a number of occasions (as shown in [16]). It is the idea, that in these cases air layers with focussing effects are slowly moving up and down, seemingly driven by surface waves. Fluctuations in intensity are not so much caused by wave chopping, because the beams do not touch the waves at all. These waves may generate in higher sea states local droplet clouds, obscuring part of the time the beam. The paper quantifies the magnitude of the effects just mentioned. In addition some consideration will be given to other effects, dealing with the target (aspect angle and height) and the sensor (fill factor and noise). Finally the effect of diffraction at wave edges and more in general the coherence of the source in view of its dimension and range will be considered.

## 2. EXAMPLES OF SIGNAL FLUCTUATIONS

In this section data are presented concerning typical signal fluctuations, as collected during various measurement campaigns in recent years. General information about the examples, with some relevant weather data, is listed in Table 1. The table shows a variety of environmental conditions, various seasons and times of the day. Most of the time the target consisted of a source with heated ceramic elements and cylindrical reflectors, providing a large beam width in horizontal direction and about 10° in vertical direction. Two of these sources were mounted in a mast, about 7-10 m above the deck of a boat, one emitting forward and one emitting backward. This boat made in- and outbound runs, making the source to appear and disappear over the horizon. The target in Duck was a small one-engine propeller plane. In Livorno the exhaust of a helicopter was used as source, while in Den Helder the helicopter carried a special 360° source on a 30 m cable, simulating a supersonic sea-skimming (SSS) missile. On Oahu the source was mounted on a big floating platform on the ocean, while at the IJsselmeer trial the source was fixed to the ground on the other side of the lake. The ranges, shown in the table, are ranges, at which for the given target height, the apparent height is just up to a few pixels in the image-plane of the camera above the horizon. In all cases the cameras were operating in the 3-5  $\mu\text{m}$  IR band: Amber Radiance 1T and Radiance HS, provided with a 100 or 250 mm lens, Milcam XP and Thermacam PM200 both with a 100 mm lens. In all cases the visibility was more than 20 km.

Table 1. List of measurements, where scintillation data were collected

Location	Date	Time (local)	Temp (air) °C	Temp (sea) °C	Wind (m/s)	Waves pp (m)	Type of target	Range (km)
Nettuno (It)	10 Jul '98	05.52	20.4	24.0	≈ 1	≈ 0.2	boat +	23.5
Duck (NC)	02 Mar '99	13.42	12	7	5	1	plane	≈ 20
Baltic (Sw)	11 May '99	15.37	4.5	4.5	≈ 4	≈ 0.5	boat +	18.6
Curaçao (NA)	11 Oct '99	07.39	27	27	3	≈ 0.5	boat +	24.7
Livorno (It)	17 May '01	10.01	18.6	18.0	4.7	0.4	helo	46
Oahu (HI)	29 Aug '01	20.30	26.3	27.0	7	1.5	FLIP +	16.4
IJsselmeer (NI)	15 May '02	10.43	13.5	14.0	7	≈ 0.5	fixed +	19.5
Den Helder (NI)	21 Jan '03	14.40	7.5	4.5	8	2	helo +	32

In Figures 1A – 1H typical recordings of signal fluctuations are presented for each of these experiments. In the plots, the signal is given as the Difference of the Sum (DOS) of the bit values of pixels in a small area around the target and a neighboring background area of the same size. Attention was spent on avoidance of saturation of the signal, which was grabbed with an 8-bits pulsar frame grabber directly from the video output. Initially the signals were recorded on SVHS or DVCAM video recorders with sufficient video bandwidth. Along the horizontal axis, the frame number is given for a total of 400 frames, equivalent to time-span of about 16 seconds. It is noted that in most cases the target intensity was spread out over a few pixels in horizontal direction as the FPA's all had 256x256 detector elements and the frame grabber has 512 pixels per line. In vertical direction the even and odd frames are displayed in an interlaced manner in one total frame. The systems were calibrated with point sources and extended sources with known temperatures and size. The S/N ratio was sufficient in all cases in order to neglect the noise compared with the fluctuations of the signal, due to scintillation effects. The figures show very strong signal fluctuations from zero to three times the average contrast. In all cases the target disappears in one or more frames and in most cases the DOS contrast obtains negative values in some frames, due to fluctuations in the background radiance in small areas, just above the horizon. The maximum signal levels come close to or even exceed the "free space" signal level. It is clear that in most cases the signal shows very low frequency behavior, as if the target disappears behind the horizon. Close observation of the video image makes it clear that this is not the case. In these cases no beams were capable to find a light path towards the narrow pupil of the sensor because of the presence of an unfavorable temperature gradient in the lower part of the atmospheric boundary layer.

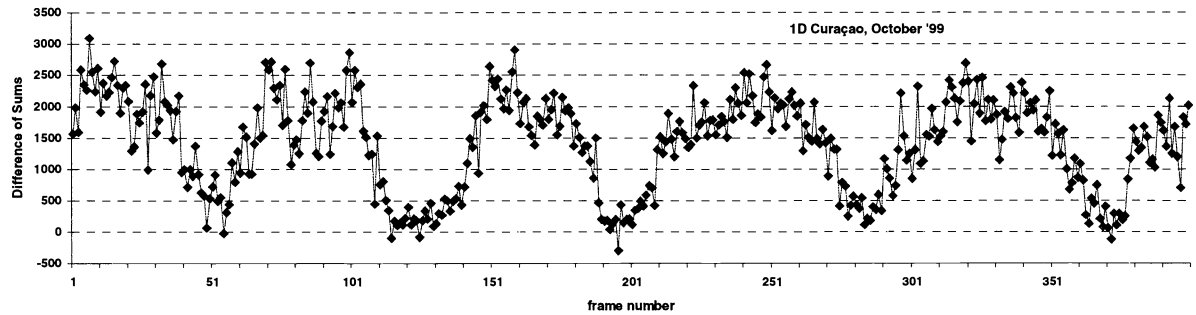
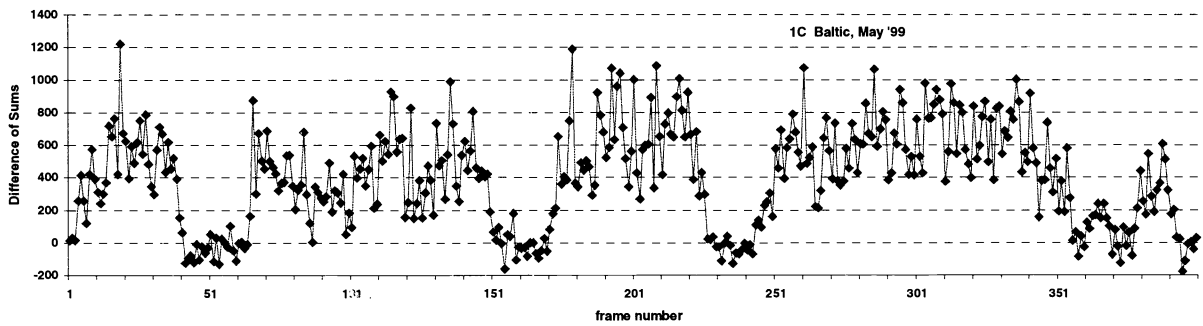
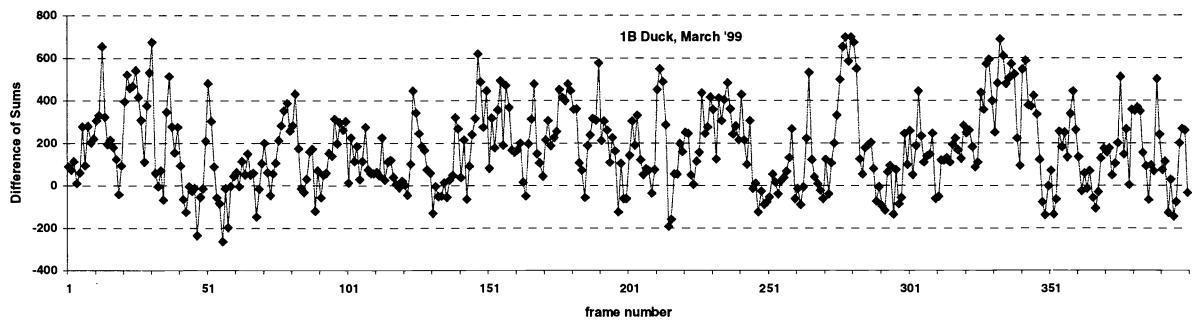
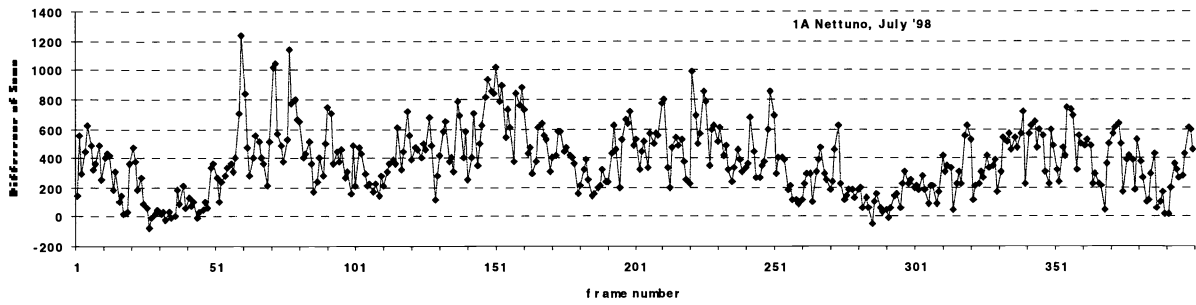


Figure 1A to 1D, Intensity fluctuations during various experiments, listed in Table 1; 400 frames  $\approx$  16 seconds

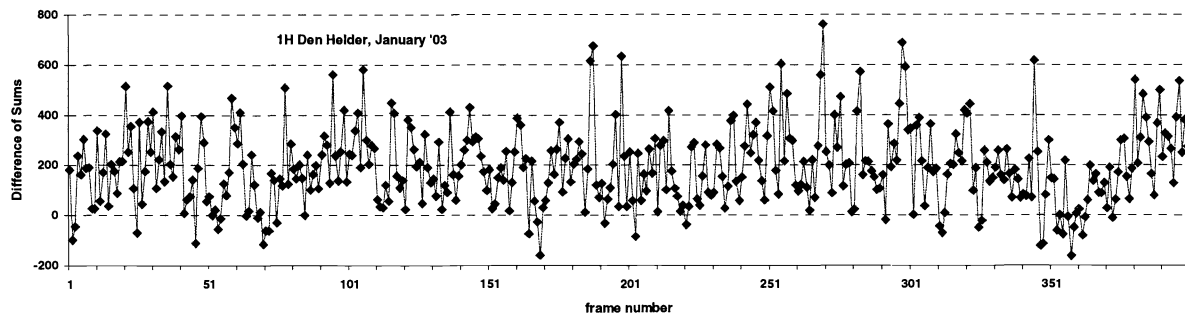
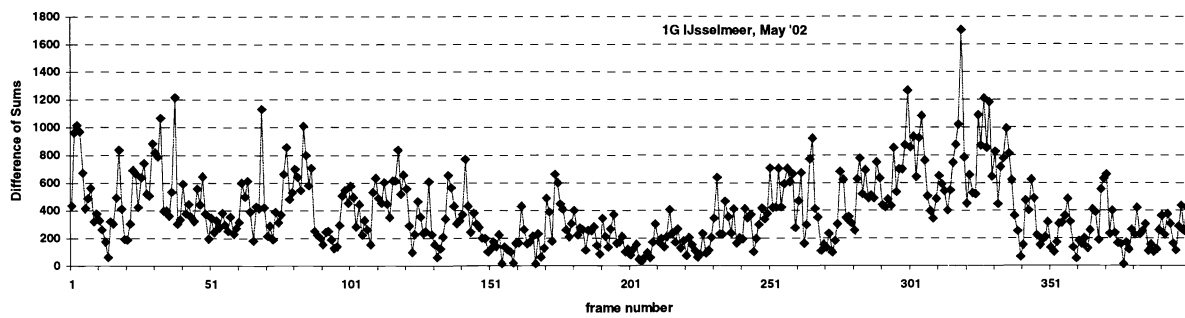
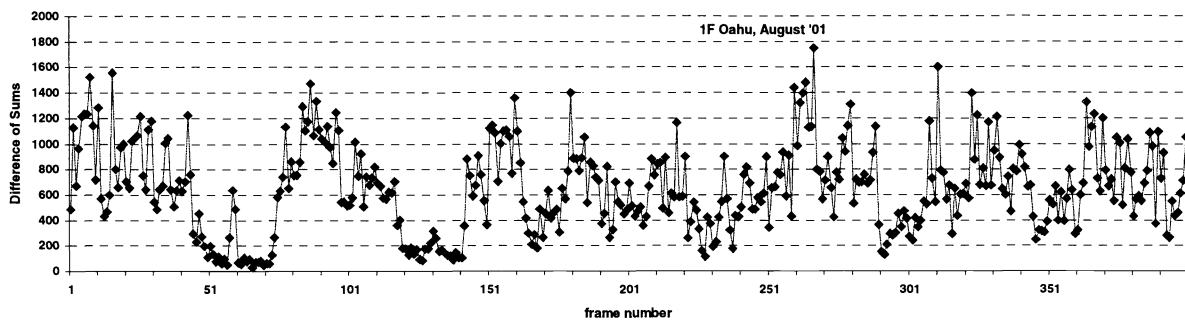
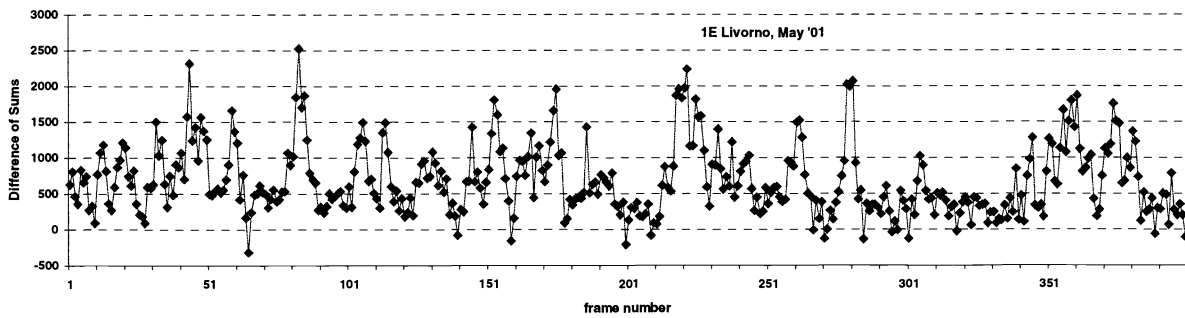


Figure 1E to 1H, continuation of results from various experiments, listed in Table 1; 400 frames  $\approx$  16 seconds

For longer ranges the percentage of the time of disappearance becomes bigger, either because the probability of finding a light path, penetrating to the pupil, becomes smaller, or sub-refraction forbids the presence of beam formation towards the pupil. An example of an image of a point target near the horizon is given in Figure 2 with the helicopter and the SSS source at a range of 32 km near Den Helder, imaged with the Radiance HS camera with 250 mm lens, providing an Instantaneous Field of View (IFOV) of 0.12 milliradian (mr). The source was hanging a few meters above the apparent horizon. It is noted that the signal fluctuations of the helicopter were bigger than those of the SSS source.

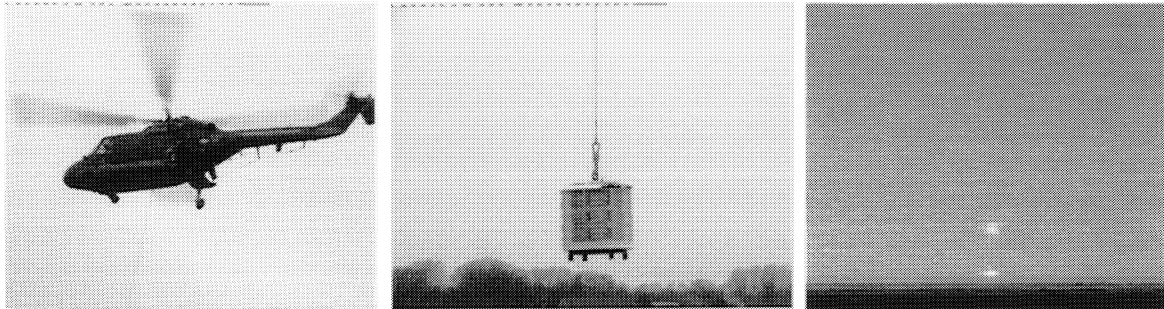


Figure 2. Pictures of the Lynx helicopter (left) with SSS source on a 30 m cable (middle) and both in the IR at a range of 32 km (right), imaged with a Radiance HS camera with 250 mm lens

### 3. EXAMINATION OF DIFFERENT PHENOMENA

#### 3.1 Coherence

For the targets of consideration in this paper, the diameter is assumed to be between 0.3 and 1.0 meter. The thermal radiation of such a source, emitted at wavelengths between 4 and 10  $\mu\text{m}$ , can be described as coming from a large number of very small centres. The phase of the waves, emitted by each of these centres, are fully uncorrelated, which means that in a pupil at a point at short range of several hundred meters, a large number of waves are arriving with a strong variation in phase. At such a range these variations avoid the occurrence of interference, when the diameter of the pupil is more than about one millimetre. The target radiation can be considered as incoherent in this case. For long ranges however (more than 10 km) the situation becomes different (see figure 3). In an isotropic medium (upper picture), a spherical wave  $W_s$ , emitted by a source  $S$ , has become a plane wave  $W_p$  at long range. Waves, emitted by other points of the source are all parallel to  $W_p$  to within an angle of  $D/R$ , where  $D$  is the diameter of the source and  $R$  the range.

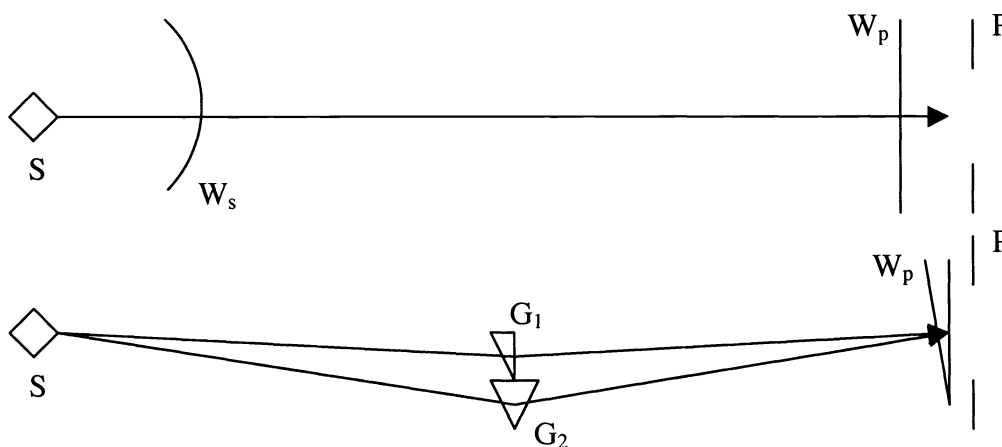


Figure 3. Illustration of coherence resulting in interference at receiving apertures P at long range due to atmospheric refraction; S = source,  $G_1$ ,  $G_2$  = temperature gradient 1 and 2,  $W_s$  = spherical - and  $W_p$  = plane wave-front

If for D and R, values of 0.5m respectively 20 km are taken, the maximum tilt of the wave-fronts is 1/40 milliradian. When the pupil of the sensor has a diameter of 40 mm, the maximum path difference over the pupil is 1  $\mu$ m, which is 1/4 of the wavelength of 4  $\mu$ m, sufficient for interference patterns, being nearly co-located for all points of the target. The bottom picture of figure 3 shows what may be the consequence in case of atmospheric refraction effects. Consider two gradients  $G_1$  and  $G_2$ , symbolized by two prisms, resulting in different deviations of the wave-fronts in the atmosphere. The two prisms act similar to the bi-prism of Fresnel, well known from classical optical interference experiments. Two wave-fronts  $W_p$  arrive at the pupil P, where they cause interference effects with horizontal fringes of high and low intensity. It is noted that waves, coming from different parts of the source, propagate through different atmospheric layers and thus the interference patterns may differ. The two wave fronts, entering the pupil, produce a mirage (two bright spots) in the focal plane of the sensor. The angle of arrival between the two spots will be the same as the angle between the two wave-fronts, for example 0.2 milliradian. In this case the distance between two fringes will be 200 mm for a wavelength of 4  $\mu$ m. It is possible in such cases, that the pupil is located in the dark area of a fringe and that the sensor receives very little irradiance from the source. One can imagine, that due to fluctuations in the layering structure of the atmosphere along the path, the interference pattern runs back and forth over the pupil, resulting in intensity fluctuations.

It is noted that both paths in the bottom part of figure 3, may have a different path-length. As long as this difference is less than about 50 cm (shorter than the coherence length of the waves), the interference patterns will continue to exist. It is also noted that for different wavelengths the distance between the fringes is different. This causes a reduction of fringe contrast, especially in the 8-14  $\mu$ m band. In the 3-5  $\mu$ m band, the main part with low molecular extinction is between 3.6 and 4.1  $\mu$ m, so the fringes will be sharper in this band. In this context, it is worth-while to consider, what the effect of a small temperature difference is on the optical path length, or what path-length is needed to create a path difference of one wave-length. For this consideration one may use the approximate formula for the refractive index of air at height h n(h) as function of temperature T and pressure p:

$$n(h) = 1 + 0.786 * 10^{-6} * p/T \quad \text{from which follows:} \quad dn = - 0.786 * 10^{-6} * p/T^2 * dT \quad (1)$$

For a temperature T = 290K and a pressure of  $10^5$  N/m<sup>2</sup>, the value of n(h) becomes 1.00027, while for a temperature difference dT of 1K, the value of dn becomes  $0.94 \cdot 10^{-6}$ , resulting in a path difference of one wave-length (4  $\mu$ m) for a path length of 4.3 m. If the gradient of 1K occurs over a width of 4 cm, the tilt of the wave-front is 0.1 milliradian over this path-length. For a path-length of 20 km, the wave-front in the warmer (lower n) air may have advanced thousands of wavelengths over the wave-front in the cooler air (higher n).

### 3.2 Target aspect angle and height

This is important issue in real scenarios where incoming weaving air targets are considered. Hot metal parts from the motor compartment and exhaust gases may be visible at certain parts of the trajectory. The sources that were used during the experiments, could only give problems, when mounted in the mast on a boat, having a pitch with amplitude of more than 5°, beyond which the radiant intensity decreases gradually. This pitch motion was generally not reached, as the boat did not go out in severe sea states. Similarly the up and down motion of the boat, causing height variations of the source, was generally limited to about 20 cm (peak-peak). This basically can have an impact on the measured signal, as the gradient of the temperature can change considerably over this distance and thus the light path (see also section 3.6). It is noted that the height of the boat source is about 40 cm, so a vertical motion of the boat of 20 cm cannot switch the received intensity on and off. When the helicopter is used as target, there may be a severe problem for certain types when they are used in front aspect, in which case the body may screen the exhausts. Small yaw motions may introduce strong intensity variations. When using the helicopter as target, a backward aspect is generally recommended, although in this case the rear part of the helicopter can cause shielding in some cases. Moreover the tail rotor can cause high frequency modulations of one of the exhausts. When the helicopter is used in daytime with presence of the sun, sun-glints on the canopy tend to be modulated by the main rotor. In both cases there may be an interference of the sampling by the camera and the modulations by the rotors.

### 3.3 Sensor fill-factor

When the sensor under consideration uses an FPA, having discrete detectors with a certain amount of un-sensitive area between the elements, it is called under-sampled. If a point target is imaged on this FPA and the optical system has a very small PSF, most of the focussed energy may well fall between two detector elements, resulting in a low signal value. The

maximum signal occurs when the point source is imaged just at the centre of a detector element. Generally the optical PSF will not be smaller than the distance between two detector elements and theoretically diffraction by the aperture will always result in some energy distribution to neighbouring detector elements. In figure 4 two extreme cases are shown with an FPA with a rather low fill-factor (about 50%). The circles  $C_1$  and  $C_2$  symbolize a small respectively large PSF. Due to atmospheric turbulence or rapidly changing refraction conditions, wave-fronts can instantaneously be tilted, resulting in lateral displacements of the circles over the detector array. Due to these displacements, signal variations occur, called here FF-scintillation. For circle  $C_1$  integrated signal fluctuations between about 25% and 100% may occur, while for circle  $C_2$  the integrated signal fluctuates a few percent around the 50% level. Payne [21] gives a more quantitative description of the phenomenon. In practice the fill-factor is much higher than in the example of figure 4. Many FPA's have fill-factors above 80%. Generally the optical PSF has a Gaussian type of shape, of which the tails are spread most of the time over an area of at least  $3 \times 3$  pixels. Furthermore when the signal is observed in the analog channel (on a TV monitor), the limited video-bandwidth adds an additional blur in the horizontal direction, diminishing further the FF-scintillation effect. Finally the position of the detector near the focus plays an important role, as defocussing increases the blur and decreases the FF-scintillation.

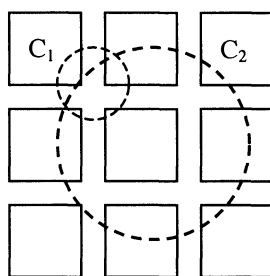


Figure 4. Illustration of fill-factor effect as source of signal fluctuations, when imaging point targets through a turbulent atmosphere over long path-lengths.  $C_1$  and  $C_2$  are different PSF's

### 3.4 Sensor noise

In general, sensor noise for FPA's consists of temporal noise for each of the pixels and of spatial noise, which manifests itself as non-uniformities due to differences in offset and gain between the FPA elements. These non-uniformities are residual after a process of non-uniformity correction (NUC), which is carried out regularly. The temporal noise is not correlated to the atmospheric scintillation effect and can just be added linearly. The total of both temporal noise and scintillation is obtained by taking the root of their sums. It is reminded that in the DOS procedure an area around the target is taken. The total temporal noise for the area is the noise of one element divided by a factor, equal to the root of the number of pixels in this area. Thus the S/N ratio is roughly improved with this factor. The spatial noise contributes to intensity fluctuations, when the target is moving rapidly over the field of view of the camera, or when the camera is panning over the scene. In the first case the differences in gain and offset appear as possible source of signal fluctuations, while in the second case the static background clutter is modulated by the non-uniformities. It is noted, that in this section it is assumed that the fill factor is 100%; otherwise a combination of the effect, described in section 3.3 will occur.

### 3.5 Diffraction by wave-tops

It is well known that light can be diffracted at edges. Although sharp edges are generally not present in a maritime environment, wave tops may act as such. A plane wave, coming from a long-distant point source, will produce a certain irradiance in the shadow area behind the edge. Figure 5, taken from classical optical literature, shows the distribution of intensity as function of the angle behind the edge, made with the line between the source and the edge. The figure is valid for a wavelength of  $0.5 \mu\text{m}$  and the horizontal scale is in milliradian. Just at the geometrical shadow line (at G), the intensity is  $\frac{1}{4}$  of that in the directly irradiated directions. In these directions the intensity fluctuates somewhat with the angle. For infrared wave-lengths around  $4 \mu\text{m}$ , the angle between the line of sight to the edge and the direction where the intensity ratio becomes 1 (line H-K), is about 3.2 milliradian. For a range of 10 km this means a height difference of about 32 m. A sensor, positioned just above the shadow line, will thus receive considerable less irradiance compared to a sensor at higher location. The irradiance fluctuations due to changing height of the wave-tops up-to 1 m will be limited to

about 10%. In view of the refraction effects in the boundary layer, it is questionable if there will be any wave-front, coming from the source, which grazes the wave-tops and enters the pupil, located at the apparent horizon. Generally the wave-fronts which are diffracted, will arrive at higher locations due to sub-refraction.

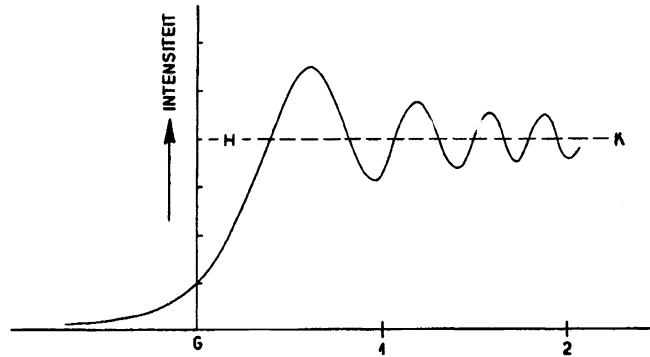


Figure 5. Illustration of diffraction of a plane wave at a straight edge (after “van Heel”); G = geometrical shadow

### 3.6 Variable layer height

In this section, an atmospheric boundary layer with a vertical temperature gradient will be assumed. This is most of the time occurring due to solar fluxes, emission to the cold sky, evaporation and wind effects at or near the surface. As an example, the function, describing the temperature  $T$  as function of height  $h$ , will be  $T(h)=T(0)+z/a*(\exp(-ah)-1)-0.006h$ . When  $z$  and  $a$  are equal, a negative ASTD of 1 °C will result. The slope of the temperature drop-off is determined by  $a$ . For ray tracing the variation of the gradient  $dT/dh$  and the associated gradient of the refractive index  $dn/dh$  with height (in m) is more relevant. In this case the following relationships are taken:

$$dT/dh = -z*\exp(-ah) - 0.006 \quad \quad \quad dn/dh = -9.35*10^{-7}(dT/dh + 3.48*10^{-2}) \quad (2)$$

in which the value 0.006 dedicated to the adiabatic temperature drop with height and the value  $3.48*10^{-2}$  is following from the drop of pressure with height.

In this example it will be assumed, that the height of the layer is moving up and down along the path from the source to the receiver, as if waves are tilting it. For this purpose another height parameter  $p$  is introduced, which relates to  $h$  by means of the formula:

$$p - h = w_1 * \sin (2\pi * j * \Delta / L_1 + \varphi_1) + w_2 * \sin (2\pi * j * \Delta / L_2 + \varphi_2) \quad (3)$$

in which  $w_1$  and  $w_2$  are wave amplitudes,  $L_1$  and  $L_2$  wavelengths,  $\varphi_1$  and  $\varphi_2$  the phase of the waves. In the ray-tracing calculation a step  $\Delta$  in forward direction is taken, while  $j$  is the step number. The procedure implies the calculation of the curvature of the ray for each step  $j$ , while the slope is adapted to the slope of the previous step (for further details see [23]). In this procedure no finite layering structure is taken;  $T$  and  $dT/dh$  are continuous functions of  $h$ . The ray-tracing provides two transfer functions for a point source in the entrance pupil at the receiver plane. The first is the arrival height  $h_e$  as function of the starting angle  $u$  with the horizon at the source and the second is the angle of arrival  $v$  versus  $h_e$ . The variations in  $v$  over the entrance pupil lead to a variation in position of arrival in the focal plane. A number of values for  $u$  are taken in order to include the lowest arrival heights of rays at the receiver plane, corresponding to the first moment of detection after popping-up of a target over the horizon. Examples of the two transfer functions are given in Figure 6A and 6B, while for the parameters the following values were chosen:  $z = a = 2.5$ ,  $w_1 = w_2 = 0.5$ ,  $\Delta = 10$  m,  $\varphi_1 = \varphi_2 = 0$ ,  $L_1 = 100$  m,  $L_2 = 1000$  m. The point source is located at a height  $h_0$  of 12.8 m and the receiver is located at a distance of 25.6 km. The total number of steps for  $j$  along the path is 2560, while  $u$  starts at an angle of  $-0.001475$  radian and 290 rays were traced, each with a step of  $1 \mu\text{rad}$ , which for free space implies a displacement of 25.6 mm at 25.6 km range.

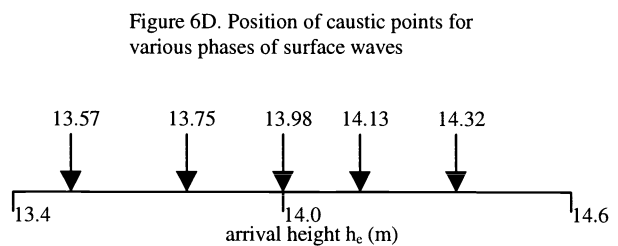
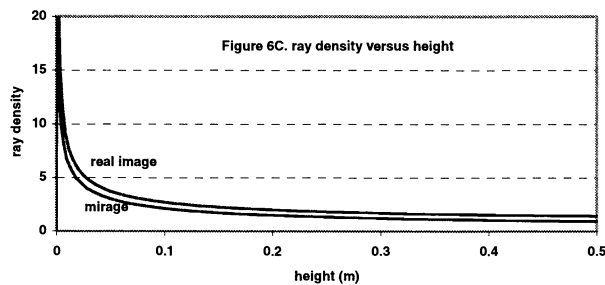
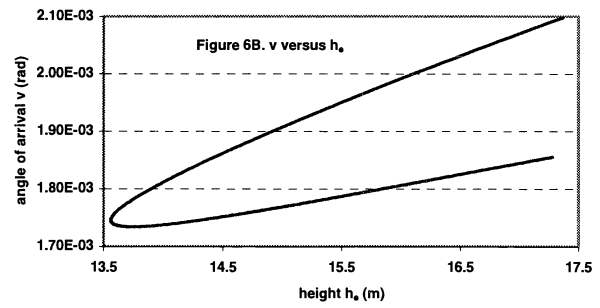
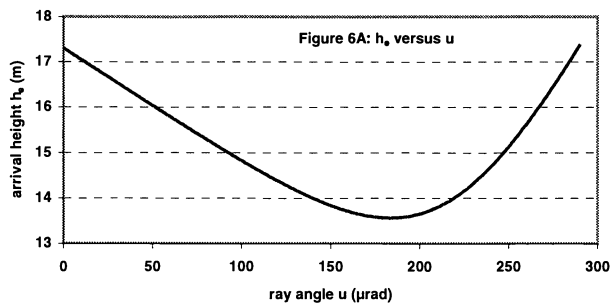


Figure 6A and B: Transfer functions of  $h_e$  versus  $u$  and  $v$  versus  $h_e$ ; 6C: normalized ray density versus  $h_e$ ; 6D: caustic intersection points in receiver plane for various  $\varphi_1$  and  $\varphi_2$  ( $0^\circ$ ,  $0^\circ$  to  $180^\circ$ ,  $180^\circ$ ), shown in meters above sea

The curves in figures 6A and 6B show the normal sub-refractive behaviour with a minimum arrival height of 13.57 m in the receiver plane and a mirage in the zone above that height. The area just above the minimum arrival height is the caustic zone, where the ray density increases tremendously, as shown in figure 6C. The ray density (for the point source) was calculated by taking the value of  $0.0256 * ( | 1/(dh_e/du)_n | + | 1/(dh_e/du)_m | )$  at each point of the transfer function. The subscripts m and n denote the mirage respectively the normal rays. The ray density would correspond to the irradiance did occur as described in section 3.1. The area with high density of just a few cm is smeared out due to the finite dimensions of the source. In the case of our example the source and the receiver are about symmetrically positioned compared to the point of contact of the earth grazing beams, so the source dimension is roughly projected inversely in the receiver plane. A source with a size of 20 cm is thus blurred as a spot with high intensity of about 20 cm. When various phases  $\varphi_1$  and  $\varphi_2$  are taken, different minimum arrival heights are found, as indicated in figure 6D. This means that when an aperture is placed somewhere in the receiver plane, the collected number of rays varies very strong, depending on the size of the aperture. The resulting signal variations will have a low frequency behaviour as the motions of the surface wave is a relatively slow process.

### 3.7 Wave chopping

In addition to the disturbance by refraction effects, wave-tops can directly reduce the irradiance level, depending on the height  $p$  of the source and the diameter  $D$  of the receiver. The highest wave-top and its location along the path count in this case. The reduction factor  $f_r$  for a homogeneous atmosphere, taking a sharp geometrical shadow at the wave-tops, ranges gradually from 1 to 0. The wave-top, located at a range  $s_1$  from the receiver, moves up over a total range  $z_0$ , equalling  $(s_1/s)*(p-D)+D$ , where  $s$  is the range between source and receiver. As the geometrical shadow is not sharp because of diffraction, the reduction factor will be less. The probability of the intensity fluctuations depends on the wave statistics. These statistics are determined by the location of the path and the sea state: shallow water in coastal areas or deep ocean with long swells. If some waves exceed the others with a height difference of about 50 cm, then the effect may be significant. These conditions may be considered as higher sea states. It is noted that the wave chopping will

generally be an irregular effect in time, as the phase of the wave-tops is irregular. During the experiments, presented in this paper, the sea state was generally low and the receiver was located considerably higher than the source. Therefore the wave chopping would have been perceived as a slow on/off switching process. This was not really found to be the case; in Curaçao (figure 1D) the signal changed from minimum to maximum within a fraction of a second.

### 3.8 Droplet clouds

In very high sea states and wind speeds, droplets, bubbles, foam and other particles are generated at the sea surface in the neighbourhood of wave crests. In this case the visibility and IR transmission go down tremendously, especially in the lower part of the boundary layer. In this case the atmosphere can be considered rather homogeneous and the extinction coefficient, even without rain, can be  $1 \text{ km}^{-1}$  and higher. For somewhat less severe conditions, the generation of particles is more local and a non-uniform atmosphere may result. One example is the generation of particles in the surf zone, of which good data are collected during the EOPACE experiments [22]. The question is, if such inhomogeneities due to particle clouds can occur and if fluctuations in apparent intensity and/or blurring may be the result. Assuming a path length of 20 km, there may be underway a number of 50 wave tops, generating particles. If each particle cloud has a diameter of 20 m, the total length of the obscuring particle zone, if connected, would be 1 km. This would result in a transmission of  $1/e$  or about 0.37, using an extinction coefficient of  $1 \text{ km}^{-1}$ . If the number of clouds varies from 40-60, the transmission varies from 0.30 - 0.45. This variation is much less than the fluctuations in intensity, found during the measurements. The contribution of temporal inhomogeneities in particle concentration along the path, is therefore considered to be of minor importance.

## 4. DISCUSSION AND CONCLUSIONS

The phenomena, described qualitatively and quantitatively in section 3 may be compared with the experimental data from figure 1. This analysis shows that some phenomena are more dominant than the other. Table 2 summarises briefly the various effects, their magnitude and probability of occurrence. The big issues for the conditions presented in this paper, are clearly the interference effects and the fluctuations in the layer along the path. In most cases a combination of effects will occur, while the different contributions are not easy to separate. Of course the magnitude of the effects is dependent on the configuration of the sensors and their signal to noise ratio. Similarly the configuration of the target determines greatly the magnitude of the signal fluctuations (the size, beam divergence and height variations).

Table 2. Comparison of various phenomena, responsible for apparent intensity variations of point targets

phenomenon	magnitude	probability of occurrence
coherence	large	high
target aspect angle and height	large	low
sensor fill-factor	small	low
sensor noise	small	low
diffraction by wave-tops	small	high
variable layer height	large	moderate/high
wave chopping	moderate	low
droplet clouds	small	moderate

It may be concluded that for obtaining more precise information on the behaviour of signal fluctuations outside the regime of inner-scale scintillation [24], which is the case in our applications, future experiments should include a fixed source and receiver with variable aperture and height. In this way one may scan the boundary layer. Furthermore precise measurement of the variation of the temperature gradient along the path is strongly recommended.

## REFERENCES

- [1] Arie N. de Jong et al, *Enhanced IR point target detection by atmospheric effects*, SPIE Volume 4820, Infrared Technology and Applications XXVIII, Seattle, July 2002
- [2] Arie N. de Jong et al, *IR panoramic alerting sensor concepts and applications*, SPIE Volume 5074, Infrared Technology and Applications XXIX, Orlando, April 2003
- [3] Robert R. Beland, *Propagation through Atmospheric Optical Turbulence*, The Infrared and Electro-Optical Systems Handbook, SPIE Optical Engineering Press, Volume 2, Chapter 2, 1993
- [4] Peter Davis et al, *IRTool: anIRST X windows Analysis Tool*, SPIE Proceedings, Infrared Systems: Design, Analysis, Modelling and Testing VI, Orlando, April 1995
- [5] Ken L. Davidson et al, *Verification of the bulk method for calculating overwater optical turbulence*, Applied Optics, 20, 2919-2924, 1981
- [6] Gerard J. Kunz, *A bulk model to predict optical turbulence in the marine surface layer*, TNO report FEL-96-A053, April 1996
- [7] J. Luc Forand, *The L(W)WKD Marine Boundary Layer Model Version 7.09*, DREV report DREV-TR-1999-099, September 1999
- [8] J. Luc Forand et al, *An extensive analysis of low-level IR transmission measurements over a 15 km path during Eopace with IRBLEM*, SPIE Volume 3433 Propagation and Imaging through the atmosphere II, San Diego, July 1998
- [9] Gerard J. Kunz, *Validation of a bulk turbulence model with thermal images of a point source*, SPIE Volume 2828, Image Propagation Through the Atmosphere, Denver, August 1996
- [10] Gerrit de Leeuw et al, *Atmospheric effects on detection of point targets at long ranges*, TNO report FEL-95-A311, July 2000
- [11] Piet B W. Schwering et al, *Infrared scintillation effects over sea*, SPIE Volume 2471, Propagation and Remote Sensing IV, Orlando 1995
- [12] T. L. Klein et al, *Characteristics of 3-5  $\mu\text{m}$  scintillation at low altitudes in a coastal marine environment*, Proceedings IRIS "Specialty Group on Targets, Backgrounds and Discrimination" Jan/Febr 1996, Albuquerque, NM
- [13] D. L. Marable et al, *Incorporation of scintillation in Infrared Detection and Track Models for Low Altitude Targets in a Marine Environment*, Proceedings IRIS "Specialty Group on Targets, Backgrounds and Discrimination", Jan/Febr 1996, Albuquerque, NM
- [14] Hubert Beaumont et al, *Experimental analysis of image quality for horizontal overwater propagation*, SPIE Volume 2828, Image Propagation Through the Atmosphere, Denver, August 1996
- [15] Arie N. de Jong et al, *Low elevation transmission measurements at EOPACE, Part III: Scintillation effects*, SPIE Volume 3125, Propagation and Imaging through the Atmosphere I, San Diego, July 1997
- [16] Arie N. de Jong et al, *Point target extinction and scintillation as function of range at LAPTEX, Crete*, SPIE Volume 3125, Propagation and Imaging through the Atmosphere I, San Diego, July 1997
- [17] Arie N. de Jong et al, *Scintillation measurements during the EOPACE November '96 and August '97 campaigns*, SPIE Volume 3433, Propagation and Imaging through the Atmosphere II, San Diego, July 1998
- [18] Arie N. de Jong et al, *TG16 point target detection experiment POLLEX, Livorno 2001*, SPIE Volume 4820, Infrared Technology and Applications XXVIII, Seattle, July 2002
- [19] Ed H. Takken et al, *Observation of IR Source at Ocean Horizon*, Proceedings IRIS "Specialty Group on Targets, Backgrounds and Discrimination", January 1995
- [20] Paul Frederickson et al, *Near-Surface Scintillation ( $C_N^2$ ) Estimates from a Buoy Using Bulk Methods during EOPACE*, Proceedings NATO-AC/323(SET) TP/2-Symposium, Naples, March 1998
- [21] Timothy M. Payne, *Apparent scintillation of subpixel targets imaged by focal plane arrays*, Opt. Eng. **36**(1) 102-108 (January 1997)
- [22] Filip P. Neele et al, *Aerosol Production in the Surf zone and Effects on IR Extinction*, Proceedings NATO-AC/323(SET) TP/2-Symposium, Naples, March 1998
- [23] Arie N. de Jong, *Refraction effects of atmospheric inhomogeneities along the path*, SPIE Volume 5237, Optics in Atmospheric Propagation and Adaptive Systems VI, Barcelona, September 2003
- [24] Guy Potvin et al, *Modelling Scintillation with Analytic Functions*, Defence R&D Canada Technical Report DREV TR 2001-060, November 2001